In Silico Optimization of Atrial Fibrillation-Selective Sodium Channel Blocker Pharmacodynamics

Martin Aguilar-Shardonofsky,[†§] Edward J. Vigmond,[††] Stanley Nattel,[¶‖**△*] and Philippe Comtois[‡△]
[†]Department of Medicine, [‡]Department of Physiology, Institute of Biomedical Engineering, and [§]Montreal Heart Institute Research Centre, University of Montreal, Montreal, Canada; [¶]Faculty of Medicine, [‖]Department of Pharmacology, and **Department of Medicine, McGill University, Montreal, Canada; and [††]Université Bordeaux 1, Institut LYRIC, Bordeaux, France

ABSTRACT Atrial fibrillation (AF) is the most common type of clinical arrhythmia. Currently available anti-AF drugs are limited by only moderate efficacy and an unfavorable safety profile. Thus, there is a recognized need for improved antiarrhythmic agents with actions that are selective for the fibrillating atrium. State-dependent Na^+-channel blockade potentially allows for the development of drugs with maximal actions on fibrillating atrial tissue and minimal actions on ventricular tissue at resting heart rates. In this study, we applied a mathematical model of state-dependent Na^+-channel blocking (class I antiarrhythmic drug) action, along with mathematical models of canine atrial and ventricular cardiomyocyte action potentials, AF, and ventricular proarrhythmia, to determine the relationship between their pharmacodynamic properties and atrial-selectivity, AF-selectivity (atrial Na^+-channel block at AF rates versus ventricular block at resting rates), AF-termination effectiveness, and ventricular proarrhythmic properties. We found that drugs that target inactivated channels are AF-selective, whereas drugs that target activated channels are not. The most AF-selective drugs were associated with minimal ventricular proarrhythmic potential and terminated AF in 33% of simulations; slightly fewer AF-selective agents achieved termination rates of 100% with low ventricular proarrhythmic potential. Our results define properties associated with AF-selective actions of class-I antiarrhythmic drugs and support the idea that it may be possible to develop class I antiarrhythmic agents with optimized pharmacodynamic properties for AF treatment.

INTRODUCTION

Atrial fibrillation (AF) is the most common type of sustained cardiac arrhythmia (1). AF is associated with reduced quality of life and increased morbidity and mortality (2). Antiarrhythmic drugs have long been used to treat AF (1), but the use of antiarrhythmic agents has markedly decreased because of limited drug efficacy and the risk of serious complications, particularly ventricular proarrhythmia (2–5). In animal and mathematical models, Na^+-channel blockers terminate AF by increasing the excitable gap and promoting the extinction of arrhythmia-maintaining rotors (6–8); however, they can also increase arrhythmic mortality (9). Recent experimental data suggest that Na^+-channel blockers can be atrial-selective (10,11), causing minimal ventricular effects. Thus, there is a strong interest in the development of AF-selective antiarrhythmic drugs with optimized efficacy and safety profiles (3).

We hypothesized that we could maximize the atrial antiarrhythmic properties of Na^+-channel blockers and minimize their proarrhythmic potential by identifying pharmacodynamic parameters optimized for selective actions on atrial tissue during AF. In this work, we address the question of how the Na^+-channel blocking kinetics influences atrial selectivity and the rate dependence of block, anti-AF efficacy, and ventricular proarrhythmic potential.

MATERIALS AND METHODS

Guarded-receptor model

To simulate state-dependent sodium current (I_{Na}) block, we used the guarded-receptor model, in which a voltage-sensitive channel gate restricts drug access to and from a constant-affinity channel-binding site (12). We assumed that the Na^+-channel blocker could bind to the Na^+-channel during either the activated (A) or inactivated (I) state. The drug's binding and unbinding kinetics are described by first-order transitions, with k_A and k_I being binding rate constants from activated and inactivated states, respectively, and l_A and l_I corresponding to the unbinding rate constants (Fig. 1). We computed the fraction of channels blocked in activated or inactivated states (B_A and B_I, respectively) using the following equations:

$$I_{Na} = g_{Na}(1 - B_A - B_I)m^3hj(V - E_{Na}) \quad (1)$$

$$\frac{dB_A}{dt} = k_A[D]m^3hj(1 - B_A - B_I) - l_A B_A\, e^{-zVF/RT} \quad (2)$$

$$\frac{dB_I}{dt} = k_I[D](1 - h)(1 - B_A - B_I) - l_I B_I\, e^{-zVF/RT}, \quad (3)$$

where g_{Na} is the Na^+ conductance; B_A and B_I are the fractional activated- and inactivated-state blocks, respectively; m is the activation variable; h and j are inactivation variables; V is the membrane potential; E_{Na} is the Na^+ equilibrium potential; z is the drug charge; F is Faraday's constant; R is the universal gas constant; T is temperature; and [D] is the drug concentration (12). We assumed that $z = 0$ (uncharged drug) for the main analysis, but also considered a positively charged molecule ($z = +1$) in single-cell

Submitted September 14, 2011, and accepted for publication January 20, 2012.

△Stanley Nattel and Philippe Comtois contributed equally to this work and share senior authorship.

*Correspondence: stanley.nattel@icm-mhi.org

Editor: Randall Rasmusson.

0006-3495/12/03/0951/10 $2.00

doi: 10.1016/j.bpj.2012.01.032

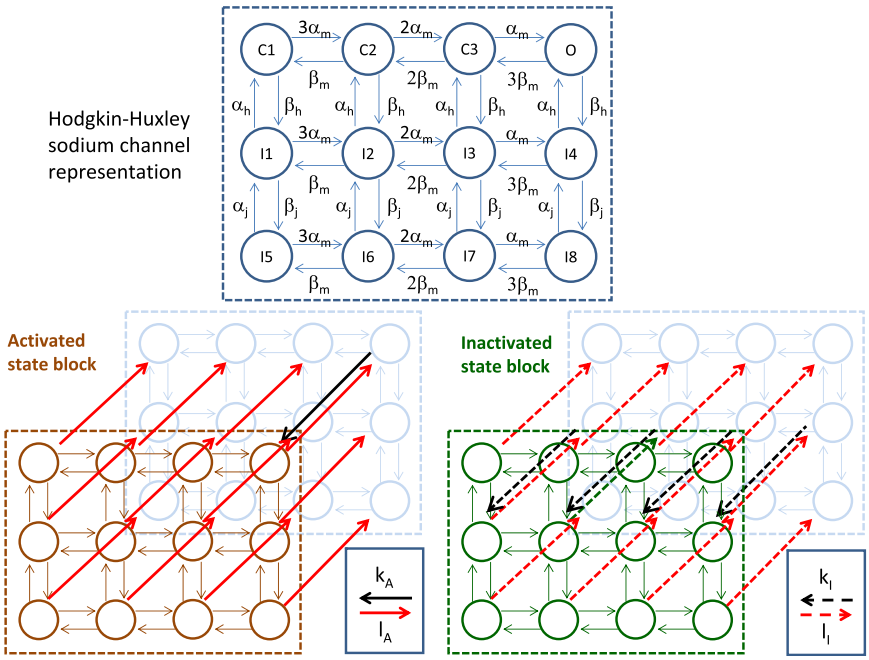

FIGURE 1 Schematic representation of the guarded-receptor model of Na^+-channel-blocking action. Transitions between the closed, activated (A), and inactivated (I) states are governed by Hodgkin-Huxley equations with rate constants α_x and β_x. Transitions between unblocked and blocked states are governed by binding-rate constants, k_A and k_I, and unbinding-rate constants, l_A and l_I.

analyses. We studied a wide range of binding and unbinding characteristics at a drug concentration of 60 μM.

Single-cell simulations

The Ramirez-Nattel-Courtemanche (RNC) ionic model of atrial cardiomyocytes (13) and the Hund-Rudy (HRd) ionic model of ventricular cardiomyocytes (14) were implemented.

The total ionic current for the RNC model ($I_{ion,RNC}$) is

$$\begin{aligned} I_{ion,RNC} &= I_{Na} + I_{K\,1} + I_{to} + I_{Kur,d} + I_{Kr} + I_{Ks} \\ &\quad + I_{Ca,L} + I_{ClCa} + I_{K,ACh} + I_{pCa} + I_{NaCa} \\ &\quad + I_{NaK} + I_{b,Na} + I_{b,Ca} + I_{b,Cl}, \end{aligned}$$

where I_{K1}, I_{to}, $I_{Kur,d}$, I_{Kr}, I_{Ks}, and $I_{K,ACh}$ are the inward rectifier, transient outward, ultrarapid delayed rectifier, rapid and slow delayed rectifiers, and acetylcholine (ACh)-activated K^+ currents respectively; $I_{Ca,L}$ is the L-type Ca^{2+} current; I_{ClCa} is the Ca^{2+}-activated Cl^- current; I_{pCa} is the Ca^{2+} pump current; I_{NaCa} is the Na^+/Ca^{2+} exchange current; I_{NaK} is the Na^+/K^+ pump current; and $I_{b,Na}$, $I_{b,Ca}$, and $I_{b,Cl}$ are the background Na^+, Ca^{2+}, and Cl^- currents, respectively (15).

The total ionic current for the HRd model ($I_{ion,HRd}$) is

$$I_{ion,HRd} = I_{Ca,t} + I_{Na,t} + I_{K,t} + I_{Cl,t}$$

with

$$I_{Ca,t} = I_{Ca,L} + I_{b,Ca} + I_{pCa} - 2I_{NaCa}$$

$$I_{Na,t} = I_{Na} + 3I_{NaK} + I_{CaNa} + 3I_{NaCa} + I_{Na,L}$$

$$I_{K,t} = I_{Ks} + I_{Kr} + I_{K1} + I_{CaK} + I_{to1} + I_{to2} - 2I_{NaK}$$

$$I_{Cl,t} = I_{to2} + I_{b,Cl}$$

where I_{CaNa} is the Na^+ current though the L-type Ca^{2+} channel, $I_{Na,L}$ is the slowly inactivating late Na^+ current, I_{CaK} is the Ca^{2+}-dependent K^+ current, I_{to1} is the 4AP-sensitive transient outward K^+ current, and I_{to2} is the Ca^{2+}-dependent transient outward Cl^- current (with other terms as defined above) (14).

RNC and HRd cardiomyocytes at 37°C were stimulated at 1 Hz (sinus rhythm frequency) and 6 Hz (AF equivalent frequency) for 3 min for each set of rate constants by numerical integration with the MATLAB ODE23s ordinary differential equation solver (The MathWorks, Natick, MA). The stimuli were 30 pA/pF 2-ms square pulses. A Na^+-channel blocker was added after 1 min and the drug effect was quantified based on a reduction in peak I_{Na} ($B_{ss} = I_{Na,CTL} - I_{Na,drug}/I_{Na,CTL}$). We changed the rate constants one at a time to study the effect of each parameter. For a fixed set of k_A and k_I, l_A and l_I were varied from 10^{-7} to 10° ms^{-1} in $10^{0.5}$ ms^{-1} intervals, generating 225 simulations for each k_A-k_I combination. The binding rate constants were then varied over k_A-k_I parameter space ($k_A = \{10^0, 10^1, 10^2, 10^3, 10^4, 10^5\}$ $ms^{-1}mol^{-1}$, and $k_I = \{1, 20, 100, 500, 2500\}$ $ms^{-1}mol^{-1}$), and for each k_A-k_I combination, l_A and l_I were varied, generating 4500 simulations each for the atrial cell paced at 1 Hz, the atrial cell paced at 6 Hz, and the ventricular cell paced at 1 Hz (for a total of 13,500 single-cell simulations). Rate-constant combinations with $B_{ss} < 50\%$ were excluded from optimization because at least 50% Na^+-channel blockade is required for AF termination (8).

We defined rate-selectivity as the ratio of B_{ss} in an atrial cell paced at 6 Hz and an atrial cell paced at 1 Hz (B_{ss} atrial 6 Hz / B_{ss} atrial 1 Hz). Atrial-selectivity was defined as the ratio of B_{ss} in an atrial cell paced at 1 Hz and a ventricular cell paced at 1 Hz (B_{ss} atrial 1 Hz / B_{ss} ventricular 1 Hz). We defined overall AF-selectivity as the product of rate-selectivity and atrial-selectivity (B_{ss} atrial 6 Hz / B_{ss} ventricular 1 Hz).

We repeated the analysis for four clinically used Na^+-channel blockers (lidocaine, procainamide, ranolazine, and flecainide) with rate constants from the literature over a clinically relevant concentration range, as follows: lidocaine: $k_A = 5173$ $ms^{-1}mol^{-1}$, $k_I = 4998$ $ms^{-1}mol^{-1}$, $l_A = 0.0128$ ms^{-1}, and $l_I = 0.0384$ ms^{-1} (16); procainamide: $k_A = 260$ $ms^{-1}mol^{-1}$, $k_I = 0.0$ $ms^{-1}mol^{-1}$, $l_A = 0.000058$ ms^{-1}, $l_I = 0.0$ ms^{-1} (17); ranolazine: $k_A = 2970$ $ms^{-1}mol^{-1}$, $k_I = 0.0$ $ms^{-1}mol^{-1}$, $l_A = 0.0053$ ms^{-1}, $l_I = 0.0$ ms^{-1} (11); and flecainide: $k_A = 5830$ $ms^{-1}mol^{-1}$, $k_I = 0.0$ $ms^{-1}mol^{-1}$, $l_A = 0.31$ ms^{-1}, $l_I = 0.0$ ms^{-1} (18).

Ventricular vulnerability simulations

We explored the vulnerable period (VP) and proarrhythmic index (PI) on a one-dimensional (1D) cable of ventricular myocytes as indices of proarrhythmic potential (19). We constructed a 10-cm cable of HRd ventricular myocytes by linking excitable segments with a 250 Ω cm axial resistivity, 100 μm length, and 11 μm radius. We stimulated the cable at 1 Hz at one end to achieve pseudo-steady-state Na^+-channel blockade after Na^+-channel blocker addition.

To measure VP, we applied a conditioning stimulus (S1) at one end and a 3-cm test stimulus (S2) 3 cm from one end. The VP was the range of S1-S2 delays that caused unidirectional propagation (20). We defined the PI as VP/(CL − RP), where CL is the pacing cycle length and RP is the refractory period (21).

Two-dimensional simulations

Two-dimensional (2D) simulations were performed on a 6.5 × 7.0 cm sheet of RNC atrial cells. The tissue contained cardiomyocyte cables (radius 5 μm, resistivity 75 Ω cm coupled by resistors (300 kΩ), length 100 μm, inserted in a brick-wall manner). Fiber resistivity and interfiber resistance values were chosen to match experimental results (15,22). AF was started by a cross-shock protocol, with S1 applied at one edge and S2 applied on a square area. The ACh effect simulated vagal tone, following a sinusoidal distribution with peak [ACh] of 15.0 nM, as previously described (8,15). We refer to the AF that continued for the full simulation (10 s) as sustained AF. Na^+-channel blockers were added at six time points (t_{DRUG} = {948, 974, 1000, 1050, 1065, 1075} ms) for every optimal rate constant combination defined by single-cell optimization, generating 120 simulations (six different t_{DRUG} values for 30 k_A-k_I combinations). Drug efficacy was expressed as the percentage of successful AF terminations for each rate-constant combination.

AF-selectivity optimization

We optimized AF-selectivity, the product of rate- and atrial-selectivity, using the single-cell analysis. We identified the l_A-l_I with maximal AF-selectivity ($l_{A,max}$, $l_{I,max}$) for each k_A-k_I combination, yielding 30 (k_A, k_I, $l_{A,max}$, $l_{I,max}$) combinations. We then used this {k_A, k_I, $l_{A,max}$, $l_{I,max}$} set to study AF termination efficacy for each of the 30 (k_A, k_I, $l_{A,max}$, $l_{I,max}$) combinations. The optimized set of binding parameters {k_A, k_I, $l_{A,max}$, $l_{I,max}$} generated little variation in the PIs because the rate-constant combinations had been selected to minimize ventricular actions. We therefore repeated the proarrhythmia analysis by fixing $l_A = 10^{-3}$ ms^{-1} and $l_I = 10^{-2}$ ms^{-1} (optimally AF-selective values in single-cell analysis), and systematically varying k_A and k_I.

RESULTS

Selectivity and binding rate constants

We first computed the drug-induced reduction in peak I_{Na} (B_{ss}) as a function of the unbinding rate constants, l_A and l_I, for a fixed set of binding rate constants, $k_A = 10^4$ $ms^{-1}mol^{-1}$ and $k_I = 20$ ms^{-1} mol^{-1} (Fig. 2, *A–C*). B_{ss} was frequency-dependent and reached almost 100% at low l_A and/or l_I. The l_A-l_I parameter space for high B_{ss} was largest for the atrial myocyte at 6 Hz, producing a region with B_{ss} that was clearly greater in atrial cells at 6 Hz than at 1 Hz. Fig. 2 *D* shows the rate-selectivity, which was greater than unity over a small region of l_A-l_I space. The maximum values for atrial-selectivity were considerably smaller than those for rate-selectivity (Fig. 2 *E*), and in no case exceeded 1.5. AF-selectivity (Fig. 2 *F*) showed a discrete area of large values, with a maximum of 5.8 at $l_{A,max}$ and $l_{I,max}$ of $10^{-3.5}$ ms^{-1} and 10^{-2} ms^{-1}, respectively.

After examining the role of unbinding (l_A and l_I), we assessed the dependency of block on binding (k_A and k_I). We first defined $l_{A,max}$ and $l_{I,max}$ as the values of l_A and l_I that maximize the AF-selectivity for a fixed k_A and k_I by varying

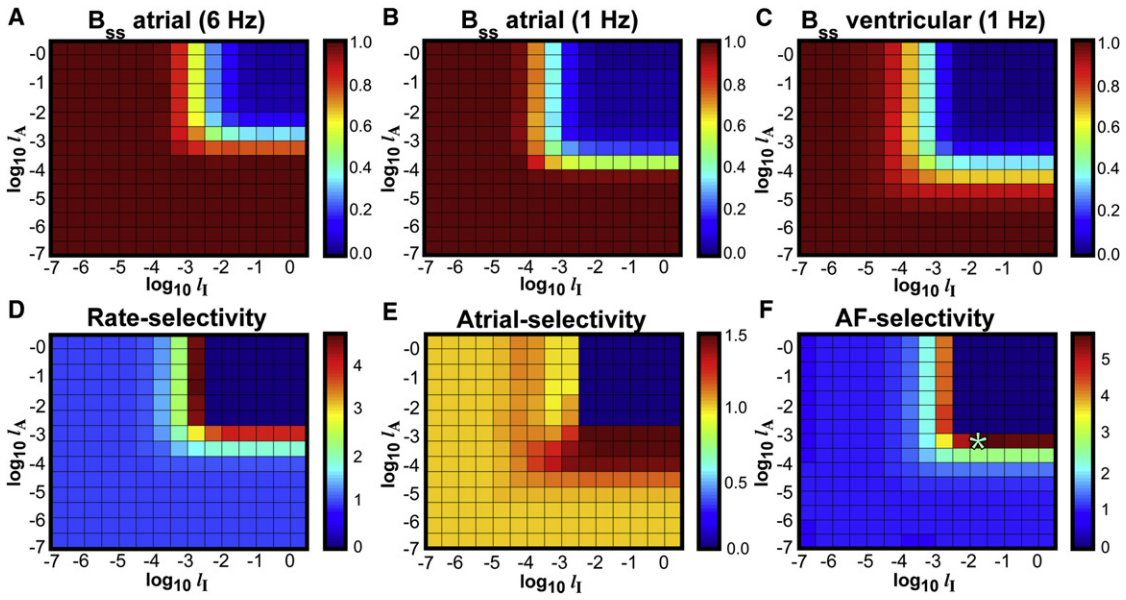

FIGURE 2 (*A–C*) Reduction in I_{Na} (B_{ss}) for an atrial myocyte paced at 6 Hz (*A*) and 1 Hz (*B*), and a ventricular myocyte paced at 1 Hz (*C*) as a function of l_A and l_I for $k_A = 10^4$ and $k_I = 20$ ms^{-1} mol^{-1}. (*D* and *E*) Rate- and atrial-selectivities. (*F*) AF-selectivity. Maximum AF-selectivity is shown by the asterisk. Color scales are at the right of each panel.

l_A and l_I independently from 10^{-7} to 10^0 ms^{-1} in $10^{0.5}$ ms^{-1} intervals. We defined AF-selectivity$_{max}$ as the AF-selectivity index at ($l_{A,max}$, $l_{I,max}$) for each k_A and k_I, varying k_A and k_I independently (k_A = {10^0, 10^1, 10^2, 10^3, 10^4, 10^5} ms^{-1} mol^{-1}, k_I = {1, 20, 100, 500, 2500} ms^{-1} mol^{-1}) to compute AF-selectivity$_{max}$ over k_A-k_I parameter space. Fig. 3, *A–C*, shows the resulting rate-selectivity, atrial-selectivity, and AF-selectivity$_{max}$. In general, rate-selectivity and AF-selectivity increased with increasing inactivated-state affinity and decreased with activated-state affinity. However, AF-selectivity fell off with increases in k_I beyond a maximum at 500 ms^{-1}mol^{-1}. The rate constants with the greatest AF-selectivity (k_A = 1 ms^{-1} mol^{-1}, k_I = 500 ms^{-1} mol^{-1}, $l_A = l_I = 10^{-2}$ ms^{-1}) had a rate-selectivity of 12.8, atrial-selectivity of 1.93, and AF-selectivity$_{max}$ of 24.6. Fig. 3, *D* and *E*, show the fraction of Na^+-channels blocked in activated (B_A) and inactivated (B_I) states for various kinetic constants, at the onset of the pseudo-steady-state action potential. Fig. 3 *F* shows B_A and B_I as a function of AF-selectivity$_{max}$. High AF-selectivity$_{max}$ values were associated with low B_A and high B_I, confirming preferential targeting of the inactivated state. The l_A and l_I values corresponding to the data in Fig. 3, *A–E*, are shown in Fig. 3, *G* and *H*, with l_A showing more variation than l_I for different k_A-k_I combinations. For comparison, results for four clinical Na^+-channel blockers are shown in Table S1 in the Supporting Material. Rate-selectivities were highest for low-dose lidocaine and procainamide, with flecainide and ranolazine being the least rate-selective. Atrial-selectivities were relatively low except for ranolazine, which had an atrial-selectivity of ~3 compared with 1.1–1.9 for the other compounds. AF-selectivities ranged from 7.8 to 15.6 for lidocaine, 7.2 to 9.5 for procainamide, 1.0 to 1.1 for flecainide, and 5.2 to 6.6 for ranolazine, and dropped off at higher concentrations for all drugs.

Finally, because ventricular proarrhythmia can arise at rates higher than normal sinus rhythm, we repeated the simulations and computed atrial-selectivity as the ratio of drug-induced reduction in $I_{Na,max}$ of an atrial cell at 6 Hz versus a ventricular cell at 2.5 Hz (Fig. S1). Optimal AF-selectivity continued to occur with inactivated-state blockers, albeit with a shift in optimal rate constants and a decrease in maximal AF-selectivity.

Fig. 4 shows atrial and ventricular action potentials (*A–C*), Na^+-current (*D–F*) and fractional block (*G–I*) in activated (B_A) and inactivated (B_I) states pre- and postdrug for the optimally AF-selective blocker (k_A = 10 ms^{-1} mol^{-1}, k_I = 500 ms^{-1} mol^{-1}, $l_A = l_I = 10^{-2}$ ms^{-1}). Effects were largest for the atrial cardiomyocyte at 6 Hz (Fig. 4, *A* and *D*). At 6 Hz, activated-state block was almost zero, whereas inactivated-state fractional block varied between 60% and 75% over the cycle (Fig. 4 *G*). At slower frequencies, inactivated-state block declined to zero over each cycle (Fig. 4, *H* and *I*).

We expanded our analysis (Fig. S2) by repeating the single-cell optimization with a positively charged molecule (z = +1) instead of a neutral molecule (z = 0). Optimal AF-selectivity continued to be associated with higher k_I and lower k_A values, but rate-selectivity and AF-selectivity were higher for the charged molecules, with maximal AF-selectivity = 89.1 vs. 24.6 for the uncharged molecule.

Ventricular proarrhythmia

We initially analyzed the proarrhythmic potential with the optimized rate constants, but found very little variation in CV and VP (Fig. S3). Because l_A and l_I had been selected

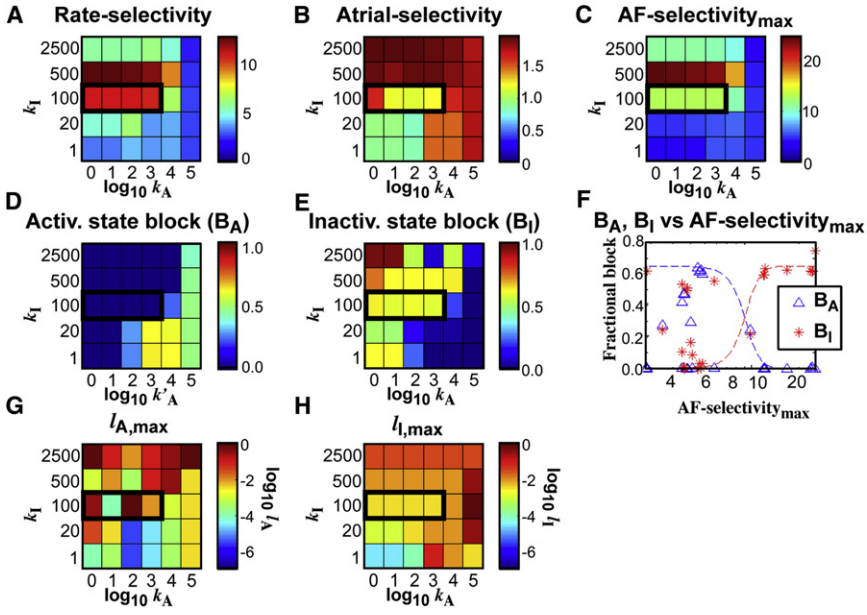

FIGURE 3 (*A–C*) Rate-selectivity, atrial-selectivity, and AF-selectivity$_{max}$ as a function of the binding-rate constants k_A and k_I. (*D* and *E*) Fractional block for activated (B_A) and inactivated (B_I) states. (*F*) Fractional block (B_A and B_I) versus AF-selectivity$_{max}$, with schematic curves (*dashed lines*). (*G* and *H*) Unbinding-rate constants ($l_{A,max}$ and $l_{I,max}$) corresponding to k_A-k_I parameter space. An area of large AF-selectivity (at k_A = 10^1–10^3 ms^{-1} mol^{-1} and k_I = 100 ms^{-1} mol^{-1}) with low proarrhythmic risk and high AF-termination rates (see Figs. 5 and 6) is shown in black boxes.

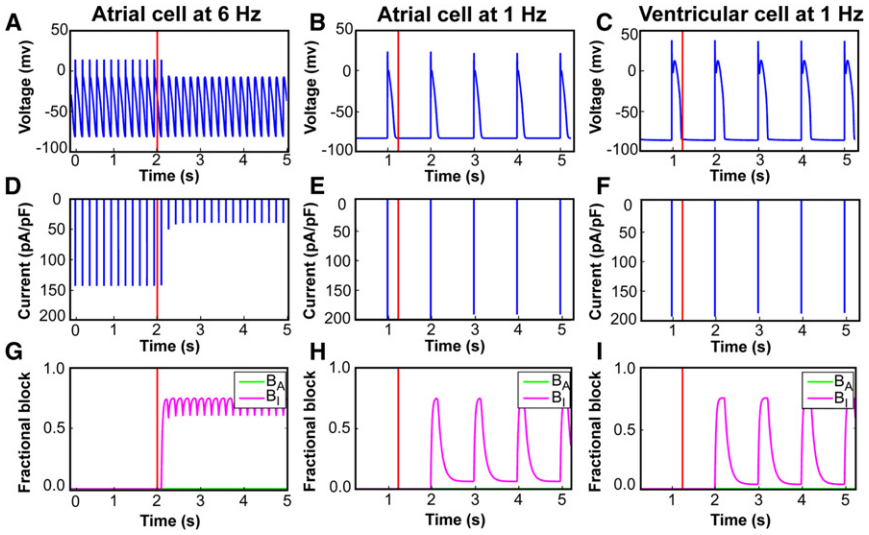

FIGURE 4 Action potentials, Na^+ current (I_{Na}), and fractional block for the optimally AF-selective Na^+-channel blocker ($k_A = 10\ ms^{-1}\ mol^{-1}$, $k_I = 500\ ms^{-1}\ mol^{-1}$, $l_A = l_I = 10^{-2}\ ms^{-1}$). (*A–C*) Effects on an atrial cell paced at 6 Hz, an atrial cell paced at 1 Hz, and a ventricular cell paced at 1 Hz. In all panels, the vertical red line corresponds to t_{DRUG}, the time at which the drug was added. (*D–F*) Corresponding values of I_{Na}. (*G–I*) Fractional block in the activated (B_A, *green*) and inactivated (B_I, *lavender*) states. Panels *H* and *I* illustrate the temporal dynamics of block: B_I rises sharply just after the action potential upstroke, corresponding to the onset of inactivation. It then reaches a plateau and starts to decrease at the end of the action potential, when the Na^+ channels recover from inactivation. B_A is negligible. The atrial cell paced at 6 Hz had a much larger B_I than atrial and ventricular cells paced at 1 Hz, because of the reduced unbinding time between action potentials.

to maximize AF-selectivity, ventricular effects were minimized. We therefore repeated the analysis, fixing the unbinding rate constants (l_A, l_I) at optimally AF-selective values ($l_A = 10^{-3}\ ms^{-1}$ and $l_I = 10^{-2}\ ms^{-1}$), varied k_A and k_I, and recomputed CV, VP, and PI. For k_A from 10^0 to $10^4\ ms^{-1}mol^{-1}$, CV was preserved, and VP and PI were minimal (Fig. 5, *A–C*). There was a sharp drop in CV (from ~55 to 39 cm/s) and increase in PI and VP (maximum increase = 55% and 32% respectively) at $k_A = 10^5\ ms^{-1}mol^{-1}$. There was little effect of k_I variations on CV, VP, and PI. Fig. 5, *D* and *E*, show B_A and B_I at action-potential onsets a function of k_A and k_I. Proarrhythmic regions with increased PI were associated with parameters that preferentially blocked the activated state (high B_A and low B_I). Fig. 5 *F* shows values of B_A and B_I at action-potential onset as a function of PI, indicating the association with B_A. CV values were little affected by the clinical drugs (Table S1) except for high-dose flecainide (39.7 cm/s).

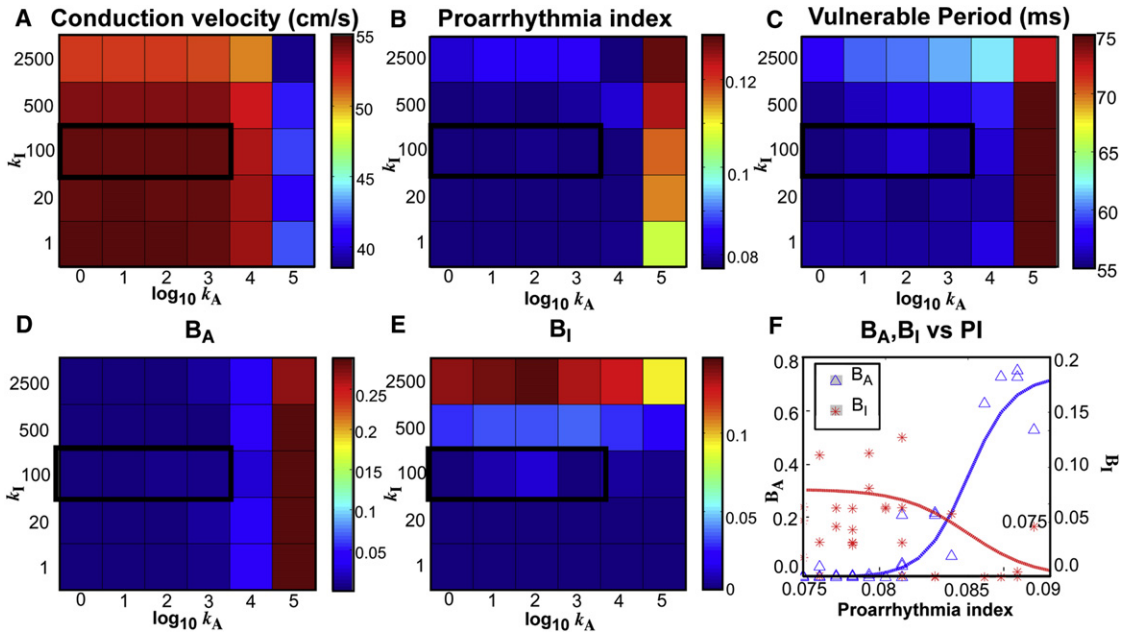

FIGURE 5 (*A*) Conduction velocity on a 1D cable as a function of k_A and k_I for Na^+-channel blockers with l_A and l_I fixed at $10^{-3}\ ms^{-1}$ and $10^{-2}\ ms^{-1}$, respectively. (*B* and *C*) PI and VP for the same parameters. (*D* and *E*) Fractional Na^+-channel block for activated (B_A) and inactivated (B_I) states in a ventricular cell at 1 Hz as a function of rate constants k_A and k_I. (*F*) Fractional block of Na^+ current in a ventricular cell at 1 Hz versus PI, with schematic curves showing that minimally proarrhythmic rate-constant combinations (low index) are associated with inactivated-state blockers, whereas proarrhythmic rate-constant combinations are associated with activated-state block. An area of large AF-selectivity with low proarrhythmic risk and high AF-termination rates (see Figs. 3 and 6) is shown in the black boxes in *A–E*.

VP was similarly little affected except for high-dose flecainide (41% increase).

Fig. S4 shows blocking dynamics for a cell in the 1D cable for four representative cases. For AF-selective k_A-k_I combinations, inactivated-state effects predominate and activated-state block is negligible, whereas activated-state block was associated with nonselective combinations.

AF termination

Termination time was smallest at high k_A and k_I (Fig. 6 *A*). Termination rates of 100% (Fig. 6 *B*) were achieved with high k_A, but also with relatively AF-selective regions (AF-selectivity ratio averaging 12.81 ± 0.07) with submaximal k_I and low k_A values, in the region shown by a black box in Figs. 3, 5, and 6. Parameter combinations in this region produced little conduction slowing (Fig. 5 *A*) or PI increase (Fig. 5 *B*). The most AF-selective area was relatively inefficient, terminating only 33% of simulations. For comparison (Table S1), lidocaine, procainamide, flecainide, and ranolazine terminated 50–67%, 0%, 16–33%, and 33–100% of AFs, respectively, over the concentration range tested. The properties of an agent with maximally AF-selective pharmacodynamics (NCB1) and an agent with submaximal AF selectivity but high AF-termination efficacy (NCB2) are also shown in Table S1 for reference.

The AF-termination mechanisms were similar to those observed in previous studies (9,19). Fig. 7 shows one example. Generators anchored in areas of low ACh concentration ([ACh]) and high action potential duration (APD; Fig. 7 *A*). Annihilation events terminated the generators but produced counter-rotating wavefronts with new generators (Fig. 7, *B* and *C*). Drug block was largest in long-APD areas (Fig. 7 *D*). The ratio of depolarized cells (R_{APD}) decreased along with the number of generators, leading to termination (Fig. 7, *D* and *E*). Fig. 8 shows AF-termination for a slightly less AF-selective but more AF-termination-efficient blocker. The mechanisms of AF-termination are qualitatively similar. A notable difference is the block dynamics, with the less-effective combination in Fig. 7 showing more beat-to-beat variation in B_T (peak-to-trough variation of 0.33) than the more-effective combination in Fig. 8 (peak-to trough variation of 0.07).

DISCUSSION

Antiarrhythmic drugs currently used for the treatment of AF have limited efficacy and insufficient safety. The potential benefits of sinus rhythm maintenance motivate a search for better antiarrhythmic drugs. Here, we used mathematical models to investigate the relationship between the pharmacodynamic properties of Na^+-channel-blocking antiarrhythmic drugs and their selectivity for atrial cells at rapid rates such as observed during AF versus ventricular cells at sinus rhythm rates. To our knowledge, this is the first study to systematically investigate the AF-selectivity of Na^+-channel blockers as a function of pharmacodynamic properties.

We found that drugs with selective binding affinity for the inactivated state are AF-selective, although selectivity is lost at very high inactivated-state affinities. We defined an optimally AF-selective region associated with maintained conduction velocity and low PI, which is relevant because decreased CV facilitates reentrant proarrhythmia (20,23,24). We also defined a non-AF-selective region (high k_A) associated with decreased CV and increased PI (Fig. 5).

The optimally AF-selective drug terminated simulated AF in only 33% of cases (NCB1 in Table S1); however, slightly less-AF-selective drugs had 100% AF-termination efficacy and low proarrhythmic potential (NCB2 in Table S1). The decrease in AF-selectivity reflects less beat-to-beat unblocking, which was important for AF-termination because, as Na^+-channel block slowed AF, beat-to-beat unblocking became pronounced and prevented termination for the most selective drugs. As tissue excitability decreases, rotor frequency and stability decrease (8,22); hence, drugs that retain efficacy at lower frequencies are able to destabilize lower-frequency rotors more effectively compared with drugs that are ineffective at lower frequencies.

One important finding is that AF selectivity does not increase monotonically with increasing inactivated-state block. Thus, drug pharmacodynamics may need to be fine-tuned to a narrow range. A possible explanation for this finding is that as k_I increases to very high values, block accumulation at lower frequencies decreases rate-selectivity and AF-selectivity.

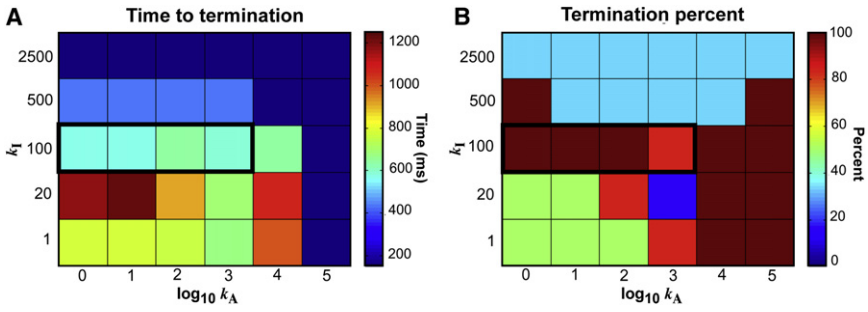

FIGURE 6 (*A*) Time to termination after Na^+-channel blocker addition on a 2D sheet of atrial cells for the same rate-constant combinations as in Fig. 3. (*B*) Percentage of successfully terminated AF episodes. The optimally AF-selective area terminated the arrhythmia quickly (average of 429 ms), although the percentage of successfully terminated simulations was lower than in the non-AF-selective region (33% vs. 100%). An area of large AF-selectivity with low proarrhythmia risk and high AF-termination rates is shown in the black boxes ($k_A = 10^1$–10^3 ms^{-1} mol^{-1}; $k_I = 100$ ms^{-1} mol^{-1}).

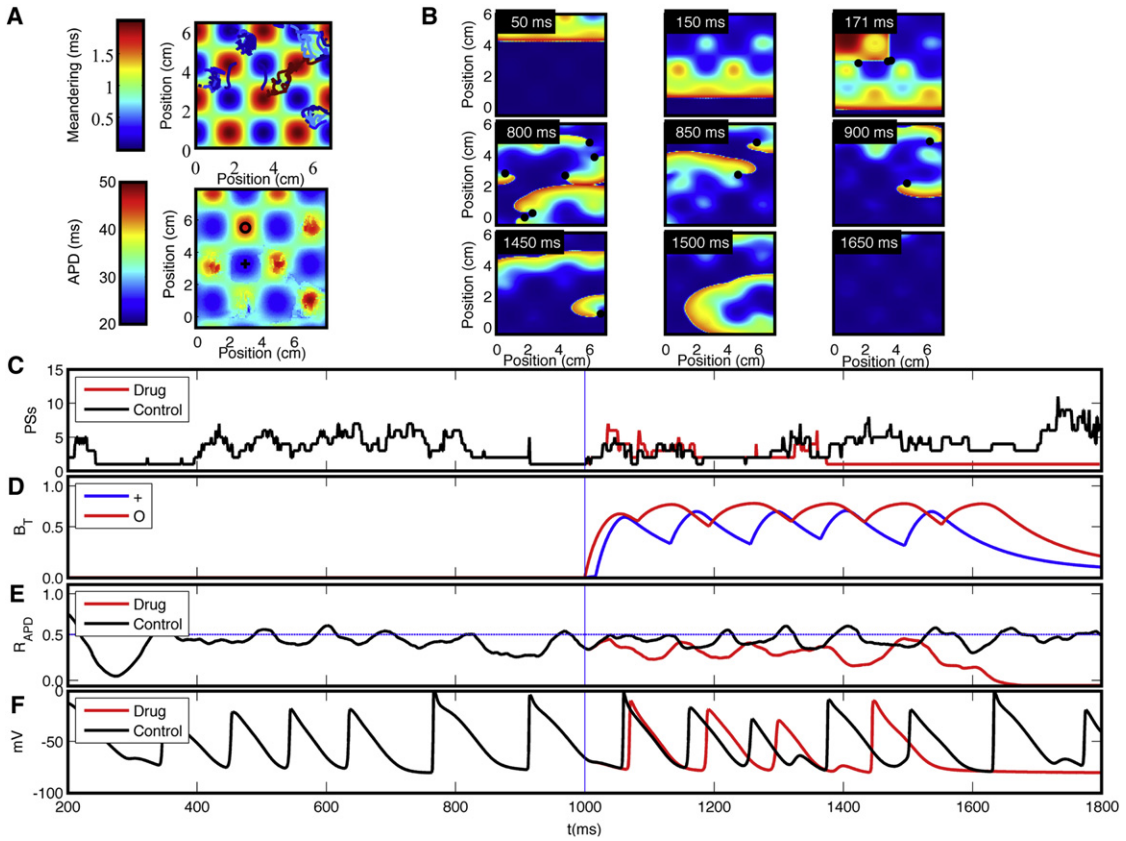

FIGURE 7 Termination of AF after addition of maximally AF-selective Na^+-channel blocker (AF-selectivity ratio = 23.9, $k_A = 10\ ms^{-1}\ mol^{-1}$, $k_I = 500\ ms^{-1}\ mol^{-1}$, $l_A = l_I = 10^{-2}\ ms^{-1}$). (*A*) Top left: Position of generators from the time of drug application ($t_{DRUG} = 1000$ ms). Bottom left: Mean APD at −60 mV (APD_{-60}) distribution. (*B*) Transmembrane potential snapshots of the 2D sheet at time points indicated at the upper left of each frame; black dots denote phase singularities. (*C*) Number of phase singularities over time in control (*black curve*) and with drug (*red curve*). (*D*) Fraction of Na^+-channels blocked at two sites (positions indicated in *A*); larger fractional block is in the region with longer APD. (*E*) Ratio of depolarized cells (R_{APD}) over time for control (*black curve*) and with Na^+-channel blockade (*red curve*). (*F*) Transmembrane action potentials over time before and after drug addition. The time of drug addition is shown in *C–F* by a vertical blue line.

According to the classical leading-circle theory, Na^+-channel blockade promotes reentrant arrhythmias by decreasing the wavelength, whereas spiral-wave theory predicts that I_{Na} blockade is antiarrhythmic (25). Previous work showed that a constant reduction in Na^+ current terminates AF by destabilizing AF-maintaining rotors (8). Comtois et al. (22) took this concept one step further by showing that a rapidly unbinding Na^+-channel blocker (lidocaine) terminates AF in a concentration-dependent manner. Here, we expand on that work by considering the relationship between Na^+-channel-binding properties and AF selectivity/efficacy. Irrespective of AF-selectivity, we found that termination occurred by previously described mechanisms, with decreased Na^+-channel availability reducing conduction velocity preferentially for wavefronts with high radius of curvature, decreasing the number of generators, and increasing meandering (6,8,22,26).

To compare our optimized drugs with clinically used Na^+-channel blockers, we repeated our analysis with reported rate constants for lidocaine, procainamide, flecainide, and ranolazine (Table S1). Lidocaine displayed the highest AF-selectivity, and flecainide displayed the lowest. Flecainide strongly decreased CV and increased VP, consistent with its known proarrhythmic potential (9). Ranolazine was the most efficacious drug and procainamide was the least efficacious, consistent with their reported clinical efficacies (27). In our single-cell analysis, the rate-constant combination with the highest AF-selectivity (NCB1 in Table S1) displayed larger AF-selectivity than the four clinical drugs but limited efficacy. A combination with slightly lower AF-selectivity (NCB2), which was twice as AF-selective as ranolazine, had 100% AF-termination efficacy.

Our findings for ranolazine are in line with the experimental observations of Burashnikov et al. (27). The non-AF-selective drug propafenone terminated vagotonic AF faster and in 100% of experiments (27), consistent with the faster and more efficacious AF-termination by non-AF-selective drugs in our simulations. Our results are also consistent with the idea that increased efficacy for AF-termination can come at the price of increasing proarrhythmic potential: flecainide is effective for AF but has significant proarrhythmic potential (28).

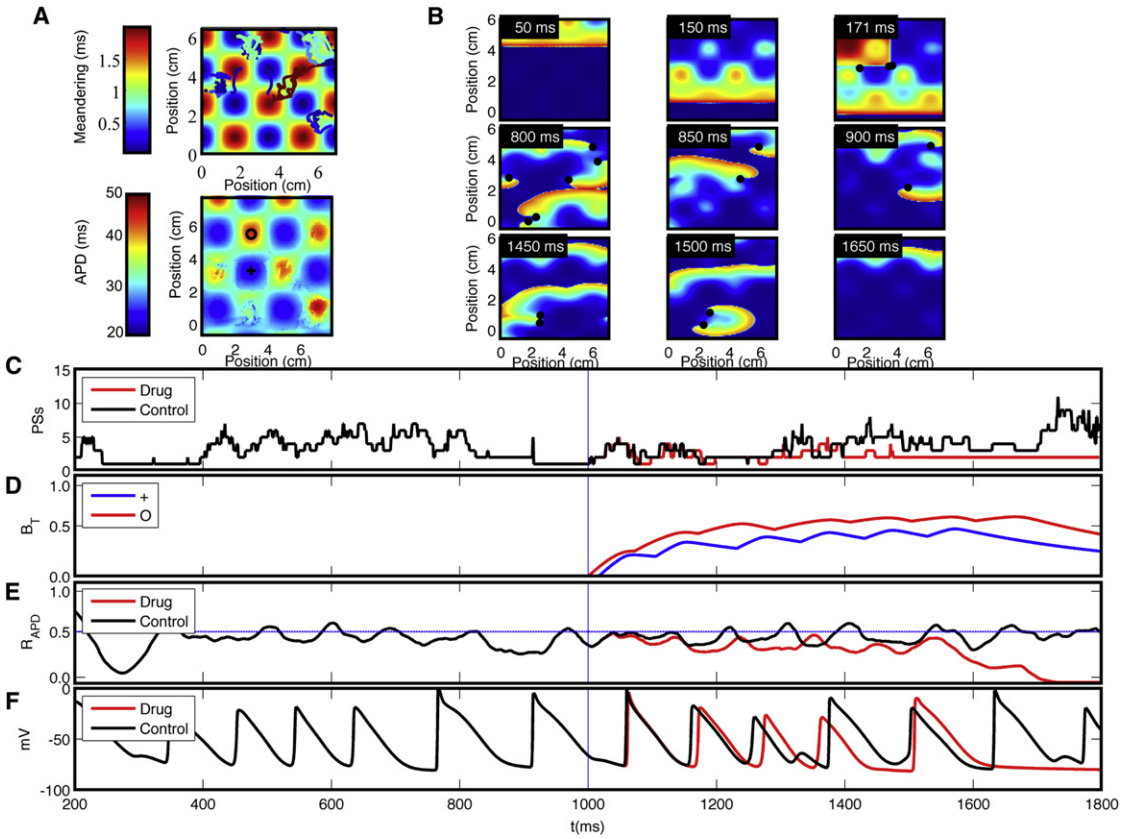

FIGURE 8 Termination of AF after addition of a slightly less AF-selective but more effective Na^+-channel blocker (AF-selectivity ratio = 12.8, $k_A = 10^2$ ms^{-1} mol^{-1}, $k_I = 100$ ms^{-1} mol^{-1}, $l_A = 10^\circ$ ms^{-1}, $l_I = 10^{-2.5}$ ms^{-1}). (*A*) Top left: Position of generators from the time of drug application (t_{DRUG} = 1000 ms). Bottom left: Mean APD at −60 mV (APD_{-60}) distribution. (*B*) Transmembrane potential snapshots of the 2D sheet at time points indicated at the upper left of each frame; black dots denote phase singularities. (*C*) Number of phase singularities over time in control (*black curve*) and with drug (*red curve*). (*D*) Fraction of Na^+-channels blocked at two sites (positions indicated in *A*); the larger fractional block is in the region with longer APD. (*E*) Ratio of depolarized cells (R_{APD}) over time for control (*black curve*) and with Na^+-channel blocker (*red curve*). (*F*) Transmembrane action potentials over time before and after drug addition. The time of drug addition is shown in *C–F* by a vertical blue line.

Ranolazine was recently shown to be an atrial-selective open-state blocker instead of an inactivated-state blocker (11). Ranolazine's atrial selectivity is thought to be based on atrial action potential characteristics, such as more negative steady-state I_{Na} inactivation voltage dependence and gradual phase-3 repolarization, as well as the rapid dissociation kinetics and steep voltage dependence of unbinding from the Na^+ channel (11,29). Of interest, we found that ranolazine, with more open-state blocking properties, was more atrial-selective than rate-selective, whereas our optimized inactivated-state blocker was more rate-selective than atrial-selective. This observation points to different mechanisms for atrial- versus rate-selectivity, which may be interesting to pursue in the future.

Overall, rate-selectivity was the major contributor to AF-selectivity selectivity in our pharmacodynamic analysis. Atrial-selectivity at 1 Hz, the ability to block the Na^+ current preferentially in atria over ventricles, ranged around unity. This finding points to a limitation of our modeling: we assumed that the drug affinities for the Na^+ channel in the atria and ventricles were identical. However, recent work suggests that Na^+ channels may differ intrinsically between the atria and ventricles (10). Our findings support recent suggestions that carefully selected class I antiarrhythmic drugs may emerge as a valid AF-selective therapeutic strategy (27,30).

Moreno et al. (18) recently investigated the in silico proarrhythmic potential of flecainide and lidocaine. Using a Markov model, they reproduced the clinically observed proarrhythmic potential for flecainide and a relatively safe profile for lidocaine, in similarity to what we found here. Of importance, in our study we did not assume any a priori pharmacodynamic properties for the compound under investigation. Instead, we analyzed Na^+-blocking drugs for AF-termination and ventricular proarrhythmia as a function of the pharmacodynamic parameter space. Thus, we were able to determine the relationship between Na^+-channel blocking properties and indices of anti-AF efficacy/ventricular proarrhythmia. Our method has the potential to contribute to rational approaches to define optimized Na^+-channel blocker properties for effective AF termination with minimized ventricular proarrhythmic

potential. It is now possible, with contemporary drug-design methods, to create candidate agents with Na^+-current blocking kinetics within a predicted range. This then raises the question: What types of pharmacodynamic properties are likely to produce the greatest likelihood of clinical efficacy with the least likelihood of proarrhythmic adverse effects? Our study provides an initial approach for identifying such optimized pharmacodynamic properties.

Study limitations

This study has a number of limitations. First, we principally considered an uncharged ($z = 0$) molecule. Use-dependent blockers are usually charged molecules (31). Because our goal in this study was to explore how the binding and unbinding characteristics of Na^+-channel blockers affect drug-selectivity, we did not analyze in detail the role of drug charge. We did repeat the single-cell simulations for a positively charged molecule ($z = +1$; Fig. S2). The results were qualitatively similar to those obtained with the uncharged drugs, except that the introduction of charge allowed for greater rate-, atrial-, and AF-selectivity. Further consideration of the charge dependence of AF-selectivity would be an interesting extension of this study.

Second, we considered a single inactivated state for the Na^+ channel. Previous work suggested that the Na^+ channel may have multiple inactivated states, and that transitions between states may not be strictly sequential; for example, a channel could transition not only from the open to the inactivated state after activation, as assumed in our study, but also directly from the resting to the inactivated state without opening (closed-state inactivation) (32). Such features could play important roles in the dynamic interaction between class I antiarrhythmics and the Na^+ channel. However, the fundamental conclusion of our study, i.e., that inactivated-state blockers are optimally AF-selective, would likely be unaffected by the inclusion of multiple inactivated states. If anything, it should be possible to achieve even greater AF-selectivity by optimizing drugs for different inactivated states, an idea that is worthy of further exploration.

Third, we used a square-pulse stimulus to pace the simulated cells. Although this is a standard stimulus that is widely used in modeling and experimental work, a square pulse does not reproduce the stimulus current shape and amplitude sensed by a cell in situ during in situ propagation, particularly during AF, where the input current waveform would likely be of longer duration and lower amplitude compared with the waveform in normal sinus rhythm. However, our findings correlate well with experimental work, and therefore we believe that our main finding would hold even if we used a more realistic stimulus.

Fourth, we used a 2D sheet with sinusoidal [ACh] variation and nonconducting boundaries to study AF-termination efficacy. This choice has the limitation of introducing geometrical biases to conclusions regarding drug efficacy (33). Indeed, the addition of Na^+-channel blocker increases meandering, leading to rotor termination on boundaries. Full exploration of this issue would require detailed analyses in accurate 3D models and is beyond the scope of this study. However, we did perform limited 3D simulations in an established model (Supporting Material), which support the main conclusions of the 2D work.

Fifth, ionic drift is an intrinsic component of mathematical action potential models that precludes true steady-state calculations (34). We ran our simulations over a relatively large number of cycles to minimize transient effects, and refer to the final state as the pseudo-steady-state to make this limitation explicit.

Sixth, we used a Hodgkin-Huxley model to simulate drug-channel interactions. However, the choice of ionic model can affect the dynamics of use-dependent block (35). We were unable to identify a canine atrial action potential model based on a Markov formulation in the literature. Full development of such a model is beyond the scope of this work. Nevertheless, a limited analysis with a ventricular-cardiomyocyte Markov model modified to reproduce our atrial action potentials at 1 and 6 Hz was consistent with our general conclusions (Supporting Material).

Seventh, we based our analysis of inactivated-state block only on interaction with the fast-inactivated state (h). However, it is possible for drugs to interact with the slow-inactivated state represented by j. To assess the impact of the j interaction, we repeated our single-cell simulations with inactivated-state block depending on combined inactivation (hj). Although there were some small quantitative differences, our overall findings remained unchanged (Supporting Material).

Finally, the pathophysiological significance of our measure of ventricular proarrhythmia, the PI, is controversial. We chose the PI because it was previously used to study proarrhythmic drug determinants (21), and it is relatively simple to define and analyze. However, the PI in a cable of normal ventricular cardiomyocytes does not reproduce potentially important components of arrhythmogenic environments in vivo, such as tissue heterogeneity and diseased myocardium, and might therefore underestimate the proarrhythmic potential in our study. It would be interesting in future work to explore the relationship between Na^+-channel blocking pharmacodynamics and more complex and clinically relevant proarrhythmia indices (e.g., arrhythmia promotion) in geometrically and physiologically realistic simulations (e.g., ischemic conditions).

CONCLUSIONS

The development of efficacious and safe antiarrhythmic agents for the prevention and treatment of AF is an important unmet need in clinical medicine. Using realistic mathematical models of atrial and ventricular cardiomyocytes, we found that Na^+-channel blockers targeting the inactivated state are more AF-selective and less proarrhythmic

than those targeting the activated state. Our findings may contribute to the effort to optimize class I antiarrhythmic drug state-dependent interactions with Na^+ channels and develop selective, safer, and effective anti-AF agents.

SUPPORTING MATERIAL

Simulations, references, two tables, and 10 figures are available at http://www.biophysj.org/biophysj/supplemental/S0006-3495(12)00114-2.

The authors thank the Réseau Québécois de Calcul de Haute Performance and Westgrid for computer resources, and France Thériault for expert secretarial assistance with the manuscript.

This work was supported by the Canadian Institutes of Health Research (MOP 44365 and 6957 to S.N.), the ENAFRA network award from Fondation Leducq (07-CVD-03 to S.N.), the Natural Sciences and Engineering Research Council (P.C.), and the Mathematics of Information Technology and Complex Systems Network (S.N. and P.C.). P.C. is a research scholar of the Fonds de la Recherche en Santé du Québec.

REFERENCES

1. Nattel, S. 2002. New ideas about atrial fibrillation 50 years on. *Nature.* 415:219–226.
2. Ehrlich, J. R., and S. Nattel. 2009. Novel approaches for pharmacological management of atrial fibrillation. *Drugs.* 69:757–774.
3. Nattel, S., and L. Carlsson. 2006. Innovative approaches to anti-arrhythmic drug therapy. *Nat. Rev. Drug Discov.* 5:1034–1049.
4. Roy, D., M. Talajic, …, A. L. Waldo, Atrial Fibrillation and Congestive Heart Failure Investigators. 2008. Rhythm control versus rate control for atrial fibrillation and heart failure. *N. Engl. J. Med.* 358:2667–2677.
5. de Denus, S., C. A. Sanoski, …, S. A. Spinler. 2005. Rate vs rhythm control in patients with atrial fibrillation: a meta-analysis. *Arch. Intern. Med.* 165:258–262.
6. Wijffels, M. C. E. F., R. Dorland, …, M. A. Allessie. 2000. Widening of the excitable gap during pharmacological cardioversion of atrial fibrillation in the goat: effects of cibenzoline, hydroquinidine, flecainide, and d-sotalol. *Circulation.* 102:260–267.
7. Kawase, A., T. Ikeda, …, H. Hirai. 2003. Widening of the excitable gap and enlargement of the core of reentry during atrial fibrillation with a pure sodium channel blocker in canine atria. *Circulation.* 107:905–910.
8. Kneller, J., J. Kalifa, …, J. Jalife. 2005. Mechanisms of atrial fibrillation termination by pure sodium channel blockade in an ionically-realistic mathematical model. *Circ. Res.* 96:e35–e47.
9. Echt, D. S., P. R. Liebson, …, CAST Investigators. 1991. Mortality and morbidity in patients receiving encainide, flecainide, or placebo. The Cardiac Arrhythmia Suppression Trial. *N. Engl. J. Med.* 324:781–788.
10. Burashnikov, A., J. M. Di Diego, …, C. Antzelevitch. 2007. Atrium-selective sodium channel block as a strategy for suppression of atrial fibrillation: differences in sodium channel inactivation between atria and ventricles and the role of ranolazine. *Circulation.* 116:1449–1457.
11. Zygmunt, A. C., V. V. Nesterenko, …, C. Antzelevitch. 2011. Mechanisms of atrial-selective block of Na^+ channels by ranolazine: I. Experimental analysis of the use-dependent block. *Am. J. Physiol. Heart Circ. Physiol.* 301:H1606–H1614.
12. Starmer, C. F., A. O. Grant, and H. C. Strauss. 1984. Mechanisms of use-dependent block of sodium channels in excitable membranes by local anesthetics. *Biophys. J.* 46:15–27.
13. Ramirez, R. J., S. Nattel, and M. Courtemanche. 2000. Mathematical analysis of canine atrial action potentials: rate, regional factors, and electrical remodeling. *Am. J. Physiol. Heart Circ. Physiol.* 279: H1767–H1785.
14. Hund, T. J., and Y. Rudy. 2004. Rate dependence and regulation of action potential and calcium transient in a canine cardiac ventricular cell model. *Circulation.* 110:3168–3174.
15. Kneller, J., R. Zou, …, S. Nattel. 2002. Cholinergic atrial fibrillation in a computer model of a two-dimensional sheet of canine atrial cells with realistic ionic properties. *Circ. Res.* 90:E73–E87.
16. Cardona, K., B. Trénor, …, J. Saiz. 2010. Exploring the role of pH in modulating the effects of lidocaine in virtual ischemic tissue. *Am. J. Physiol. Heart Circ. Physiol.* 299:H1615–H1624.
17. Villemaire, C., P. Savard, …, S. Nattel. 1992. A quantitative analysis of use-dependent ventricular conduction slowing by procainamide in anesthetized dogs. *Circulation.* 85:2255–2266.
18. Moreno, J. D., Z. Iris Zhu, …, C. E. Clancy. 2011. A computational mode to predict the effect of class I anti-arrhythmic drugs on ventricular rhythms. *Sci. Transl. Med.* 3:1–9.
19. Starmer, C. F., A. A. Lastra, …, A. O. Grant. 1991. Proarrhythmic response to sodium channel blockade. Theoretical model and numerical experiments. *Circulation.* 84:1364–1377.
20. Starmer, C. F., T. J. Colatsky, and A. O. Grant. 2003. What happens when cardiac Na channels lose their function? 1. Numerical studies of the vulnerable period in tissue expressing mutant channels. *Cardiovasc. Res.* 57:82–91.
21. Starmer, C. F. 2002. How antiarrhythmic drugs increase the rate of sudden cardiac death. *Int. J. Bifurcat. Chaos.* 12:1953–1968.
22. Comtois, P., M. Sakabe, …, S. Nattel. 2008. Mechanisms of atrial fibrillation termination by rapidly unbinding Na^+ channel blockers: insights from mathematical models and experimental correlates. *Am. J. Physiol. Heart Circ. Physiol.* 295:H1489–H1504.
23. Starmer, C. F., A. O. Grant, and T. J. Colatsky. 2003. What happens when cardiac Na channel function is compromised? 2. Numerical studies of the vulnerable period in tissue altered by drugs. *Cardiovasc. Res.* 57:1062–1071.
24. Ravens, U. 2010. Novel pharmacological approaches for antiarrhythmic therapy. *Naunyn Schmiedebergs Arch Pharmacol.* 381:187–193.
25. Nattel, S., J. Kneller, …, L. J. Leon. 2003. Mechanisms of termination of atrial fibrillation by class I antiarrhythmic drugs: evidence from clinical, experimental, and mathematical modeling studies. *J. Cardiovasc. Electrophysiol.* 14(10, Suppl):S133–S139.
26. Cabo, C., A. M. Pertsov, …, J. Jalife. 1996. Vortex shedding as a precursor of turbulent electrical activity in cardiac muscle. *Biophys. J.* 70:1105–1111.
27. Burashnikov, A., J. M. Di Diego, …, C. Antzelevitch. 2008. Atrial-selective sodium channel block as a strategy for suppression of atrial fibrillation. *Ann. N. Y. Acad. Sci.* 1123:105–112.
28. Farkas, A. S., and S. Nattel. 2010. Minimizing proarrhythmic risk in drug development and clinical practice. *Drugs.* 70:573–603.
29. Nesterenko, V. V., A. C. Zygmunt, …, C. Antzelevitch. 2011. Mechanism of atrial-selective Na^+ channels by ranolazine: insights from a mathematical model. *Am. J. Physiol. Circ. Physiol.* 201:H1615–H1624.
30. Burashnikov, A., and C. Antzelevitch. 2009. New pharmacological strategies for the treatment of atrial fibrillation. *Ann. Noninvasive Electrocardiol.* 14:290–300.
31. Hille, B. 1977. Local anesthetics: hydrophilic and hydrophobic pathways for the drug-receptor reaction. *J. Gen. Physiol.* 69:497–515.
32. Basler, J. R. 2001. The cardiac sodium channel: gating function and molecular pharmacology. *J. Mol. Cell. Cardiol.* 33:599–613.
33. Comtois, P., and S. Nattel. 2011. Impact of tissue geometry on simulated cholinergic atrial fibrillation: a modeling study. *Chaos.* 21:013108.
34. Kneller, J., R. J. Ramirez, …, S. Nattel. 2002. Time-dependent transients in an ionically based mathematical model of the canine atrial action potential. *Am. J. Physiol. Heart Circ. Physiol.* 282:H1437–H1451.
35. Liu, S., and R. L. Rasmusson. 1997. Hodgkin-Huxley and partially coupled inactivation models yield different voltage dependence of block. *Am. J. Physiol.* 272:H2013–H2022.